This journal is © The Royal Society of Chemistry 2023

Supplemental Information

BeadPak dimensions

The chamber geometry can be modified needs for the experiment or applications. The shape of the adhesive mask impacted the fluid flow. **Figure 1** depicts a couple of the designs we fabricated and tested for BeadPak. The straighter edges led to better fluid exchanges compared to the curved edges. This geometry design cut from a 360um adhesive stack resulted in a 25uL chamber.

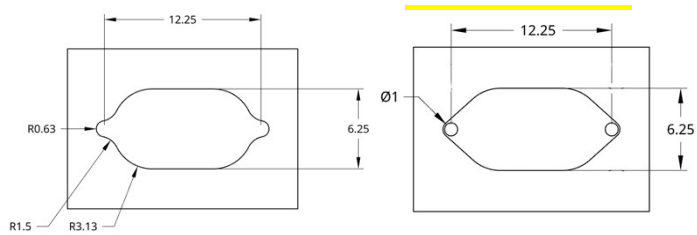

Figure 1. Dimensions of two designs tested for BeadPak chamber geometry. The design with less curves (right) proved better for fluid exchanges.

Fluid handling

The BeadPak chips were fabricated with 2 ports for fluid entry and removal. Fluid exchanges were accomplished by pipetting in or out of the ports on the lid of the BeadPak chip. During incubations, the ASAPs are driven by the magnet below to mix the fluid. **Figure 2** demonstrates how the fluid was introduced and removed from the chips. For nucleic acid assays requiring multiple fluid exchanges for capture, wash, and elution, the fluids were added and removed in this way, clearing the chamber prior to the next fluid introduction. The incubation times that were discussed in the main text were not long enough to evaporate the fluid in the chips, however when longer incubations were explored an adhesive strip was placed over the ports to prevent evaporation.

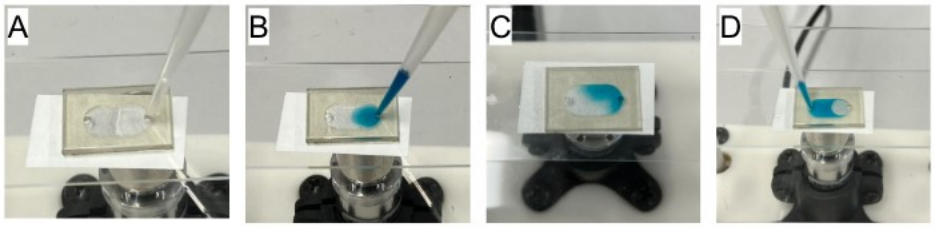

Figure 2. A-D demonstrate steps of the dye-mixing test. A. The initial solution is added to the chip. B. The dyed fluid is added to the chip. C. The magnet is turned on to actuate the ASAPs and mixing occurs. D. After the fluid is mixed it can be removed from the chip with a pipette.

Chamber height

Prior to the collection of application-specific data, we completed a coarse optimization of the chamber geometry for BeadPak chips including chamber height. We selected two chamber heights, 330 µm and 223 µm, with chamber height defined by the thickness of the adhesive mask separating the upper and lower surfaces on the interior of the chip. This was done in our well controlled streptavidin/biotin bead assay to maximize capture efficiency. Here, we found that this moderate decrease in chamber height had little to no impact on the capture efficiency (**Figure 3**). As a result, we selected the taller adhesive mask in order to minimize the x-y footprint required for any targeted chamber volume.

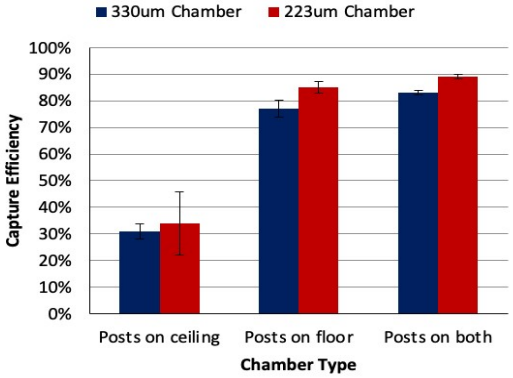

Figure 3. Moderate changes in chamber height have little impact on capture efficiency while adding Redbud Posts to the chamber floor significantly enhances capture efficiency.

Bead modification and retention

The prevention of magnetic bead loss is key to ensuring captured targets are not washed away during the fluid exchanges required for rinse and elution steps. By keeping the microfluidic chip exposed to the high field strengths of the magnetic driver we are able to retain more than 99% of beads during these exchanges. In **Figure 4** (a), we show the concentration of the magnetic bead solution loaded into the channel at the beginning of the experiment and the concentration of beads present in the recovered wash buffer (**Figure 2** (b)). In each case, the solution has been added to a hemocytometer to enable quantitative analysis of the bead solution.

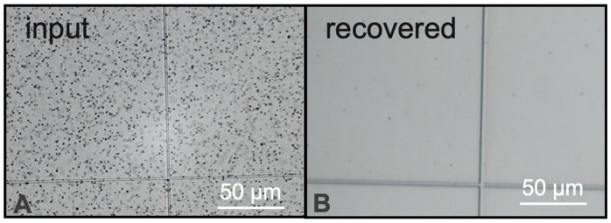

Figure 4. Magnetic beads loaded into BeadPak chips are retained during processing.

Magnetic drive optimization

Prior to the collection of application-specific data, we completed a coarse optimization of the magnetic drive system using our well controlled streptavidin/biotin bead assay to maximize capture efficiency. Field strength, and drive frequency, the speed at which the actuatable surface attached posts (ASAPs) rotate, were tested as described below. Two driver designs were utilized for this work: standard single throughput (S-drive) and high throughput (HT-drive).

Field strength: The impact of magnetic field strength was tested by adjusting the separation between the drive magnet and the ASAP array while keeping the post actuation rate (drive frequency) constant at 10k RPM. Increased field strength has been shown to cause the posts to deflect/bend farther from their upright position, thus increasing the rotational velocity of the individual posts in response to a rotating magnetic field. As seen in **Figure 5**, increasing the field strength from 100mT to our maximum of 130mT produces a significant increase in capture efficiency. As a result, data collected in the main text of this manuscript was collected using the optimal field strength. To ensure the ASAPs are exposed to the optimal field strength, they were positioned directly above the rotating magnet as **Figure 2** demonstrates. The field drops dramatically with each millimeter away from the magnet, which was ideal for designing an automated system around this component.

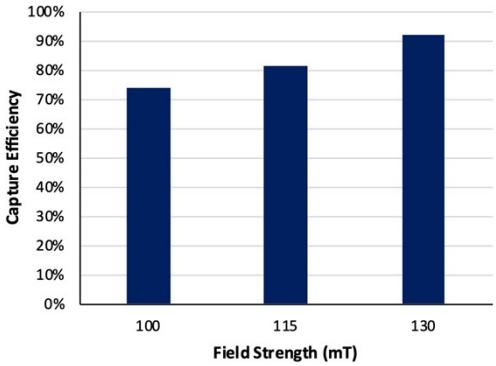

Figure 5. Capture efficiency improves at higher field strengths, corresponding to larger ASAP tilt angles.

Drive frequency: The effect of post actuation rate on capture efficiency was evaluated using a fixed magnetic field strength (**Figure 6**). Drive speed was found to positively correlate with capture efficiency, with capture efficiency increasing rapidly from the no-mix case (0 RPM) to a relatively low-rate of 2,500 RPM. Above this rate, the efficiency improves moderately and appears to plateau between 7,500 and 10,000 RPM. For this purpose of the experiments presented in this paper, we selected 10,000 RPM as the optimized actuation rate and thus used it for the collection of all data sets.

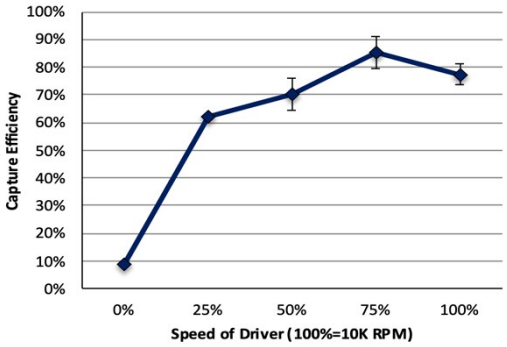

Figure 6. Capture efficiency appears to reach a plateau for actuation rates above 7500 RPM.

Driver Type: In order to simplify data collection and consistency we developed a high- throughput driver (HT-drive) capable of actuating posts in up to 6 chambers simultaneously. We've verified that this driver produces the same capture efficiency as the standard driver (S-drive) (**Figure 7**). However, there were differences in the magnets and stage design for the two driver types. In the standard driver, a diametrically magnetized (K&J Magnetics R828DIA) magnet was used and the stage was an acrylic layer with and inset for the BeadPak chip over the magnet. With this type of magnet we observed conical beat patterns of the ASAPs that resulted in mix patterns resembling a whirlpool. The HT drive employed alternating north and south (K&J Magnetics AX2C45-N and AX2C45-S) magnets and the stage could be heated to 65 Celsius, which was particularly useful for the nucleic acid protocols. When exposed to this type of driver the ASAPs produced asymmetric whip motions and the mix patterns resulted in more linear transport of the fluids from one side of the chip to the other.

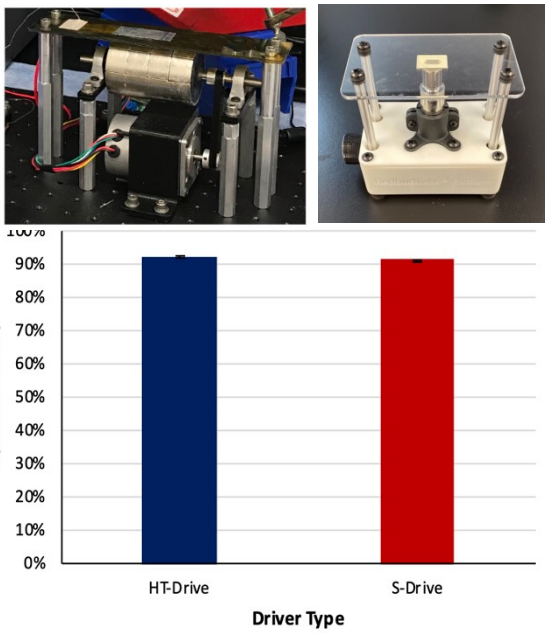

Figure 7. High-throughput driver (HT-drive, pictured left) capture efficiency is on par with that of the standard driver (S-drive, pictured right).

Fluorescent bead capture assay calibration

To determine the concentration of biotin-coated fluorescent polystyrene beads (both 1.0 µm and 0.22 µm) used in our well-controlled capture assay, we developed calibration curves relating the concentration of targets to fluorescent intensity. This data was used to define the upper and lower limits of detection for the assays, as defined by the red and blue vertical bars seen in **Figure 8** (a & b).

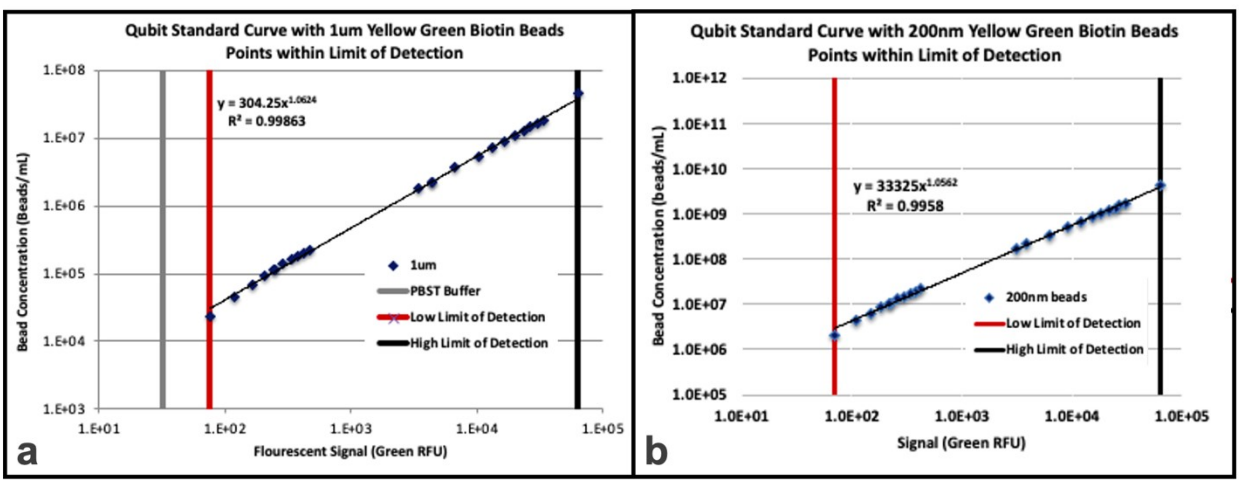

Figure 8. Calibration curves for (a) one micron and (b) 200 nanometer beads are linear over approximately 3 orders of magnitude

Nucleosome capture assay

Assay calibration: Nucleosome quantification was achieved by developing a calibration assay. The fluorescent intensity of known nucleosome concentrations in the same buffer used for experiments was determined and a calibration curve established. This calibration curve was then used to convert the fluorescent intensity from recovered nucleosome into an absolute number, so that a capture efficiency may be determined as seen in **Figure 9**.

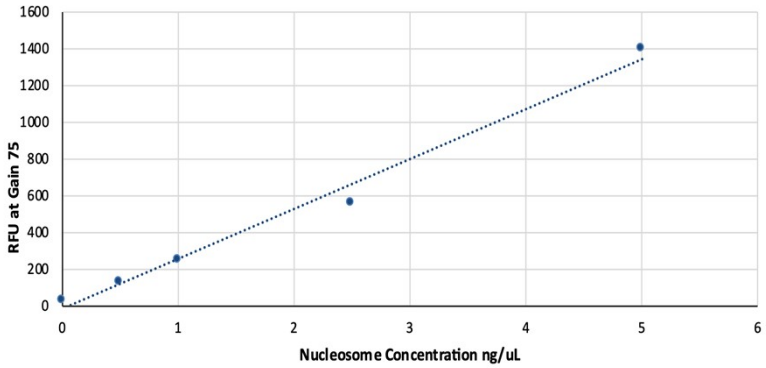

Figure 9. Calibration curve used for quantification of nucleosomes.

Tube-based assay performance: The behavior of the magnetic bead-based nucleosome capture assay was tested in tubes prior to chips to ensure validity. As seen in **Figure 10**, the performance was highly dependent upon magnetic bead concentration, with a 1 hour incubation capturing approximately half has many nucleosomes when using 0.1 mg/mL bead concentration as compared to 0.25 mg/mL bead concentration.

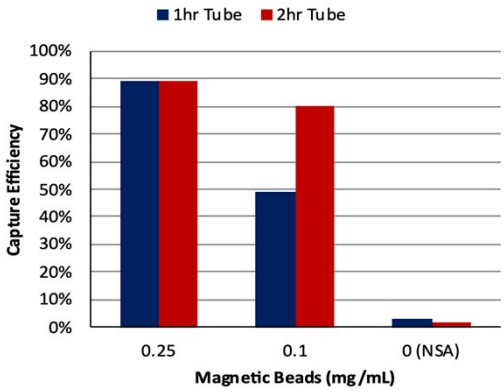

Figure 10. Higher bead concentrations reduce the time required for tube-based nucleosome capture.

Nucleic Acid Capture and Recovery

Non-MagMAX NA capture data: Various kits were used to capture and recover NA. The following table describes the performance across standard tube assays, microfluidic chips lacking ASAPs, and BeadPak chips with ASAPs. In all cases BeadPak outperformed the microfluidic setting lacking Redbud Posts. Apart from the Ampure bead kit, BeadPak chips matched or even outperformed the standard tube assays. See **Table 1.**

Magnetic bead (probe)	Target	Tube Workflows	Microfluidic chip (no RBP)	BeadPak Worklfows	Improvement over microfluidic chip	Improvement over Tube Workflows
1 micron Streptavidin	1 micron polystyrene Biotin beads	72%	8%	92%	11.5x	1.3x
2.8 micron Streptavidin]	1 micron polystyrene Biotin beads	19%	9%	66%	7.3x	3.5x
1 micron Ampure Bead kit	DNA ladder	91%	17%	75%	4.4x	0.8x
1 micron ChargeSwitch Bead kit	DNA template	97%		93%		1.0x

Table 1. Capture of targets by magnetic beads in three modes of operation: traditional testing in tubes, microfluidic chip with static ASAPs, and BeadPak microfluidic chip with actuating ASAPs. Tube workflows processed 200uL while chips processed 20uL.

ASAP Induced Shear: We have investigated the impact of actuating ASAPs for nucleic acids of different lengths to determine if posts actuating at the maximum rotational velocity (maximum magnetic field strength, maximum RPM) produce any shear-induced damage. **Figure 11** shows a DNA ladder with nucleic acid lengths ranging from 200 bp to 20 kbp that was added to a microfluidic chip containing ASAPs and incubated for 10 minutes. In the mix condition posts were actuated, while in the other condition they were static. In both cases, the distribution of nucleic acid sizes approximately matches that of the input sample (Ladder + control), indicating that significant shear induced damage is not a concern. These results are consistent with those from cell growth experiments, where it was shown that long-term exposure to actuating posts does not reduce cell counts (on the contrary, it promotes cell growth).

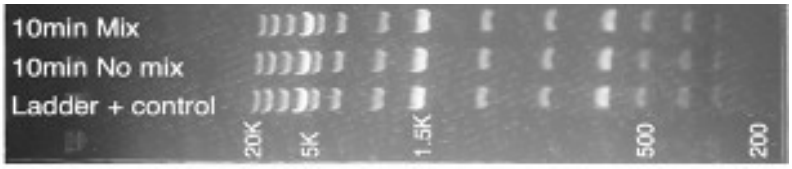

Figure 11. ASAPs do not impact nucleic acid integrity when static or actuating. Nucleic acid bands matched the control ladder that was not exposed to a BeadPak chip.

NA quantification: The concentration of recovered MS2 RNA has been determined using qPCR with the reagents and recipes in **Table 2.** The concentration of recovered E.coli DNA has been determined using PCR with the reagents and recipes in **Table 3.**

Primer Type	**Sequence for MS2**
Forward Primer	CTTCAGCAATCGCAGCAAA
Reverse Primer	GGAAGATCAATACATAAAGAGTTGAACTTC
FAM Probe	5'-/56-FAM/CAA ACA TGA GGA TTA CCC ATG TCG AAG ACA /36-TAMSp/ -3'

RT-qPCR Recipe	**µL 1x rxn**
Luna Universal probe 1 step rxn mix	10
Luna Warmstart Reverse Transcriptase	1
Forward Primer	0.8
Reverse Primer	0.8
FAM probe	.4
UDG	.5
Water	1.5
RNA sample/elution buffer	5

Cycles	**Stage**	**Time sec**	**Temp C**
1	UDG activity	120	37
1	Reverse Transcription	600	55
1	Initial Denaturation	60	95
45	Denaturation	10	95
	Extension	30	60

Table 2. This MS2 Primer sequence combination and PCR recipe resulted in consistent amplification for data reported on in the main text.

Primer Type	Sequence E. coli
Forward Primer	5'-GCA AAC TGA TGT CTT CCG CAC-3'
Reverse Primer	5'-CGA GCG GAA CAA TCA GCA T-3'
FAM Probe	5'-/56-FAM/TCA GCT GAT CAA CAC CGT TCA CGT TGA/3BHQ_1/-3'

qPCR Recipe	µL 1x rxn
Luna Universal probe 1 step rxn mix	10
Forward Primer	0.8
Reverse Primer	0.8
FAM probe	.4
UDG	.5
Water	2.5
DNA sample/elution buffer	5

Cycles	Stage	Time sec	Temp C
1	UDG activity	120	37
1	Initial Denaturation	60	95
40	Denaturation	10	95
	Extension	30	60

Table 3. This E.coli Primer sequence combination and PCR recipe resulted in consistent amplification for data reported on in the main text.

Reagent and Inhibitor Carryover: Sufficient washing and removal of inhibitors is critical for the nucleic acid isolation workflow in BeadPak. Table 4 demonstrates that BeadPak effectively reduced the urea content in an unprocessed urine sample from >300mMol down to <1mMol in the eluate, which is below the threshold for PCR inhibition. A urea detection kit (abcam #ab83362) was employed to measure urea content in the initial urine sample, and the urea remaining in the eluates of urine samples processed by two different NA isolations protocols using BeadPak: a single capture cycle of 10 minutes or 4 cycles of 5 minute capture cycles. Wash and elution were the same for both. A buffer sample was also tested to confirm that the elution buffer or exposure to the BeadPak chip was not impacting the urea detection kit. In addition to urea testing, ethanol detection kits (Fisher Scientific #50-489-254) and in house methods for detecting remnants of the lysis buffer have been used to investigate effective clearing of the buffers used in the BeadPak isolation protocols.

Sample	Urea (µM)
Urine (initial sample tested)	304427
Urine processed in BeadPak with a single 10-minute capture cycle, followed by wash and elution (eluate tested)	225
Urine processed in BeadPak with 4 cycles of 5-minute captures, followed by wash and elution (eluate tested)	332

Table 4. Urea content measured from initial urine samples compared to eluates after isolation protocol in BeadPak.